BIOCHEMISTRY
including biophysical chemistry & molecular biology
Article

Biochemistry **2009,** *48,* 3877–3886 3877
DOI:10.1021/bi802205g

Crystal Structure of Human Fibrinogen[†,‡]

Justin M. Kollman,[§,⊥] Leela Pandi,[§] Michael R. Sawaya,[∥] Marcia Riley,[§] and Russell F. Doolittle*[,§]

[§]*Department of Chemistry and Biochemistry and Division of Biology, University of California at San Diego, La Jolla, California 92093-0314, and* [∥]*UCLA Department of Energy Institute of Genomics and Proteomics, Los Angeles, California 90095*
[⊥]*Present address: Department of Biochemistry and Biophysics, University of California, San Francisco, CA 94518*

Received December 1, 2008. Revised Manuscript Received March 17, 2009

ABSTRACT: A crystal structure of human fibrinogen has been determined at approximately 3.3 Å resolution. The protein was purified from human blood plasma, first by a cold ethanol precipitation procedure and then by stepwise chromatography on DEAE-cellulose. A product was obtained that was homogeneous on SDS−polyacrylamide gels. Nonetheless, when individual crystals used for X-ray diffraction were examined by SDS gel electrophoresis after data collection, two species of α chain were present, indicating that some proteolysis had occurred during the course of operations. Amino-terminal sequencing on post-X-ray crystals showed mostly intact native α- and γ-chain sequences (the native β chain is blocked). The overall structure differs from that of a native fibrinogen from chicken blood and those reported for a partially proteolyzed bovine fibrinogen in the nature of twist in the coiled-coil regions, likely due to weak forces imparted by unique crystal packing. As such, the structure adds to the inventory of possible conformations that may occur in solution. Other features include a novel interface with an antiparallel arrangement of β chains and a unique tangential association of coiled coils from neighboring molecules. The carbohydrate groups attached to β chains are unusually prominent, the full sweep of 11 sugar residues being positioned. As was the case for native chicken fibrinogen, no resolvable electron density could be associated with αC domains.

Fibrinogen is a large, multidomain glycoprotein composed of pairs of three nonidentical polypeptide chains ($\alpha_2\beta_2\gamma_2$);[1] it is found in the blood plasma of all vertebrates. Its thrombin-catalyzed transformation into fibrin, the fundamental fabric of blood clots, has intrigued protein scientists for more than a century (*1*−*3*). Briefly, fibrin is formed when thrombin removes small peptides from the amino termini of α and β chains, exposing sets of "knobs" that interact noncovalently with ever-present "holes" on neighboring molecules to form oligomers termed protofibrils. As polymerization progresses, thrombin-activated factor XIII incorporates covalent cross-links, initially between the carboxy-terminal segments of γ chains, but eventually including α chains also. The details of how protofibrils associate to form the macroscopic fibers of the clot remain major targets for research in the field.

The intrinsic floppiness of fibrinogen has proved to be a formidable barrier to crystallization. Although numerous crystal structures have been reported for core fragments of proteolyzed fibrinogen (*4*−*16*), only the molecule from chicken has been crystallized in a native form suitable for X-ray diffraction (*17*, *18*). The success with the avian protein has been attributed to the absence of flexible high-repeat regions universally found in the α chains of mammalian fibrinogens (*19*) (Figure 1). Consistent with that supposition, a backbone structure has been reported for bovine fibrinogen treated with a lysine-specific bacterial protease that removed the carboxyl-terminal thirds of α chains, as well as the first 60 residues of the β chains (*20*).

Here we report reproducible conditions that yield diffraction-grade crystals of human fibrinogen. The conditions are similar to those used for the chicken system in that the chemical chaperone TMAO[2] proved to be an essential contributor (*21*). Although the material used for

[†]This work was supported in part by Grant HL-81553 from the National Heart, Lung and Blood Institute.
[‡]The atomic coordinates and structure factors for the new structure described in this article have been deposited in the Protein Data Bank (PDB) (entry 3GHG).
*To whom correspondence should be addressed. Telephone: (858) 534-4417. Fax: (858) 534-4985. E-mail: rdoolittle@ucsd.edu.
[1]The 1973 Nomenclature Committee of the International Society of Thrombosis and Hemostasis recommended that the three nonidentical chains be designated Aα, Bβ, and γ, where A and B represent fibrinopeptides A and B, respectively (*60*).

[2]Abbreviations: GHRPam, Gly-His-Arg-Pro-amide; GPRPam, Gly-Pro-Arg-Pro-amide; PEG, polyethylene glycol; TMAO, trimethylamine oxide; MPD, methylpentanediol; NPGB, nitrophenyl guanidinobenzoate; CNS, Crystallographic and NMR System; MR, molecular replacement; rmsd, root-mean-square deviation; SDS, sodium dodecyl sulfate; TLS, translation, libration and screw-rotation; XDS, X-ray Detector Software.

Published on Web 3/18/2009

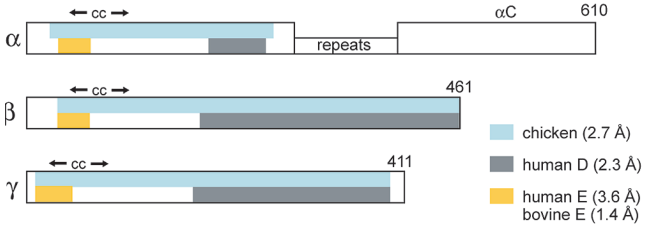

FIGURE 1: Schematic depiction of α, *β*, and *γ* chains of human fibrinogen showing regions previously determined at side chain resolution for bovine fragment E_5 (*9*), human fragments D and D-dimer (*5*, *7*), and human fragment E (*13*). The regions involved in coiled coils are denoted cc. In human fibrinogen α chains, there are ten 13-residue repeats that are absent in chicken fibrinogen. The repeat region and the αC domain are mostly disordered and cannot be discerned in electron density maps. Numbers refer to chain lengths of human fibrinogen in residues.

crystallization was homogeneous by various criteria, some incipient proteolysis occurred during the extended times needed for crystals to form and reach a suitable size, and it may be that removal of some α-chain material is in fact a requirement.

In general, the structure confirms and extends inferences made on the basis of structures from other species. In this regard, although the sequences of human and chicken fibrinogens are approximately 60% identical overall, the differences are not uniformly distributed. The *β*C and *γ*C domains that make up the bulk of previously crystallized fragments D are much more conserved and are ~80% identical. In contrast, the coiled coils that connect the distal and central domains are only ~40% identical. The flexibly attached and mobile αC domains, which cannot be identified in electron density maps, are only ~30% identical in the two species.

Some of the most interesting features emerging from the new structure involve crystal packing. For one thing, the new structures (the two molecules in the asymmetric unit differ) increase the number of possible conformations that may occur in solution, differing as they do in the bending and twisting of the coiled-coil regions. It is likely that the differences in twisting and bending observed between various structures are a reflection of unique packing forces; still, the various resulting conformations are of interest because they may parallel the real flexibility that occurs in solution. That such forces are ordinarily quite weak suggests that fibrinogen in solution, and especially in circulating blood, must be subject to a significant amount of distortion away from the canonical sigmoid structure first demonstrated by electron microscopy studies (*22*).

Beyond that, different interactions have been observed between the various domains in neighboring molecules; these are important because in the past inferences have been made about the nature of fibrin formation on the basis of packing observed in crystals of fibrin(ogen) fragments (*23*). The underlying basis for considering contact points as potential polymerization sites rests on fibrin formation being a self-assembly process that occurs spontaneously after the thrombin-catalyzed release of fibrinopeptides. A wide variety of weak interactions needs to occur over and beyond the knob−hole interactions that initiate the process for protofibrils to become associated in the fibrin network. The latter must also be sufficiently flexible to allow a cohesive network to form in any irregular tissue landscape.

Finally, the idiosyncrasies of crystal packing have provided an unprecedented glimpse of an entire carbohydrate cluster that occurs adjacent to *β*-chain holes. Mobile as these clusters may be under physiological conditions, they must hinder access by flexibly tethered B knobs during fibrin formation (*24*).

MATERIALS AND METHODS

The synthetic peptides GPRPam and GHRPam were those described in earlier publications from this laboratory (*5*, *7*, *8*) and had been synthesized by the BOC procedure (*25*).

The first step in the purification of fibrinogen involved a series of cold ethanol precipitations from human blood plasma as described previously (*26*). The second and final step used chromatography on DEAE-cellulose and was based on published procedures (*27*, *28*), except that an empirically determined stepwise elution was employed instead of a gradient. In this regard, the column was initially equilibrated with 0.039 M Tris-phosphate buffer (pH 8.6); elution was achieved with a series of increasingly concentrated Tris-phosphate buffers at pH 7.4, 6.9, 6.4, and, finally, 4.1 (Figure 2A). Protein in pooled fractions was precipitated by addition of $^1/_3$ volumes of cold saturated ammonium sulfate, redissolved in smaller volumes of appropriate buffers, and dialyzed. The material pooled from the major peak was used for crystallization. The preparation, which appeared homogeneous on SDS gels (Figure 2B), was treated with NPGB (final concentration of 50 μM) before being flash-frozen in 0.5 mL aliquots and stored at −78 °C.

Crystals were grown at room temperature in sitting drops made from equal volumes of a 9 mg/mL protein solution in 0.15 M NaCl, 0.05 M Tris (pH 7.0), and 1 mM $CaCl_2$, containing 2 mM GPRPam and 2 mM GHRPam, and well solutions composed of 0.05 M Tris (pH 7.0) containing 4% PEG-3350, 0.25−0.5 M TMAO, 1.0 mM $CaCl_2$, and 2 mM sodium azide. Typically, a precipitate formed during the first 24 h; crystals appeared in ~1 week and continued to grow over the course of 1−2 months (Figure 2C). At this point, the cryoprotectant MPD was added gradually to a final concentration of 15%, after which the crystals were frozen and stored in liquid nitrogen. Amino-terminal sequencing was conducted on crystals at the UCSD Sequencer Facility.

Preliminary X-ray diffraction data were collected at the UCSD X-ray Crystallography Facility. Higher-resolution data were collected at the Advanced Light Source (Lawrence Berkeley National Laboratory, Berkeley, CA), beamline 8.2.2. Data were processed with HKL2000, Denzo, and Scalepack (*29*), as well as with XDS (*30*). The structure was determined by molecular replacement using AMoRe (*31*), as provided in the CCP4 package (*32*), and Phaser (*33*). Model reconstructions were conducted with O (*34*); the initial refinement was conducted with CNS (*35*), and final refinements were performed with RefMac (*36*). Compositional omit maps were prepared with 10% of the residues randomly removed in an effort to minimize model bias (*37*). Structural alignments were made with the lsq operation in O (*34*) and the align command in PyMol (*38*).

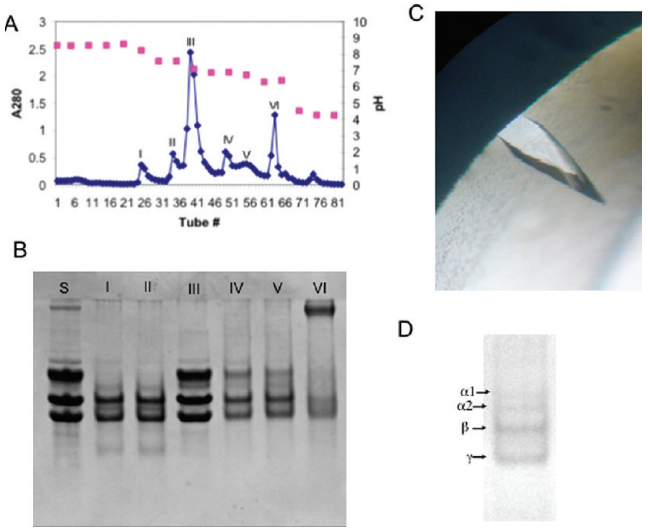

FIGURE 2: (A) DEAE chromatography of human fibrinogen that had been prepared by cold ethanol fractionation from human blood plasma. The material in pool III was used for obtaining crystals. (B) SDS gel (5% acrylamide, reducing conditions) corresponding to the starting material and the various fractions from DEAE chromatography (I–VI). (C) Photograph of the crystal of human fibrinogen used for data collection. (D) Characterization of the same crystal by SDS gel electrophoresis (5% acrylamide, reducing conditions) after data collection.

The problem of the markedly anisotropic diffraction was addressed by the process of ellipsoidal truncation (*39*). The original reflection file was passed through an online anisotropy server (www.doe-mbi.ucla.edu/~sawaya/anisoscale/anisotropy) that performed an ellipsoidal truncation of the data (*39*). Briefly, the directional bias dependence of diffraction is taken into account by constructing boundaries on reflections as ellipsoids of dimensions inversely related to the limiting resolutions ($1/a^*$, $1/b^*$, and $1/c^*$). Anisotropic scale factors were applied to correct for the anisotropy from the data, after which a negative isotropic B was applied to restore the full value of the high-resolution reflections compromised by the anisotropic scaling. A detailed explanation of the procedure appears on the server website.

The data were subjected to further refinement with RefMac (*32*) in conjunction with TLS (*40*). The coordinates of a current model were passed through a TLS server (http://skuld.bmsc.washington.edu/~tlsmd/) for optimization of TLS modules (*41*), from which 24 groups were selected (two for each of the 12 chains in the two molecules in the asymmetric unit).

Some further model manipulation was performed with COOT (*42*). Model geometries were monitored with PROCHECK (*43*). Illustrations were prepared with the aid of PyMol (*38*).

RESULTS

Protein and Crystal Purity. The protein contained in pool III from DEAE chromatography was virtually homogeneous on SDS gels (Figure 2B). It was visibly free of fibronectin and was shown by assay to lack factor XIII. During the 3–6 weeks needed to obtain large crystals, however, some minor proteolysis did occur. The principal crystal used for data collection was saved and examined by SDS gel electrophoresis (Figure 2D); it was evident that two forms of α chain were present. Both bands were smaller than the native form, consistent with known cleavage sites in α chains lacking peptides corresponding to the 27 and 56 carboxyl-terminal residues, respectively. It is possible, perhaps even likely, that minor trimming of the α chains is necessary for crystallization of mammalian fibrinogens.

Three small crystals were dissolved together and subjected to amino-terminal sequencing through five cycles. The predominant residues corresponded to the sequences of the Aα and γ chains (the native Bβ chain is blocked). There were also small amounts of pairs of amino acids consistent with the removal of fibrinopeptides A and B from some molecules, but there was no evidence of the commonly observed cleavage that exposes Alaβ43.

Data Collection and Processing. Altogether, three complete data sets were collected, including two on the same crystal. The best of these was made up of 800 images collected at 0.25° at a distance where the outermost spots would occur at 2.9 Å. The overall completeness was 92.6% to 3.3 Å resolution when all of the data were used (cutoff = 0; no weak reflections removed) (Table 1). The diffraction was distinctly anisotropic, however, as was true in the past for crystals of chicken fibrinogen (*17*, *18*) and the modified bovine fibrinogen (*20*).

Molecular Replacement. Molecular replacement was conducted with the equivalent of a single fragment D from human fibrinogen (the ABC chains from D-dimer, PDB entry 1FZC), as well as with the central region of chicken fibrinogen (PDB entry 1M1J). Although the Matthews coefficient (Table 1) indicated the presence of two molecules per asymmetric unit, implying four D fragments, only two solutions were found with AMoRe (*31*). In contrast, the MR program Phaser (*33*) was able to identify two more D fragments, as well as two central regions corresponding to two E fragments.

Model Rebuilding and Refinement. Considerable rebuilding was necessary in the four regions corresponding to the coiled coils, each of which was distinctive. To this end, a version of the chicken model coiled-coil region, mutated to the human amino acid sequence, was cut into short segments that were used as preliminary templates for fitting. The high-resolution structure of bovine fragment E_5 (PDB entry 1JY2) (*9*) was also a valuable aid in modeling the central regions.

The model was subjected to numerous cycles of modification and refinement, restraints on the ϕ and ψ angles of helical regions of the coiled coils being maintained throughout the process. Various structural features were obvious, including calcium atoms, α-chain carbohydrate clusters, and the peptide ligands, GPRPam and GHRPam.

At this point, anisotropic analysis revealed that, by the arbitrary criterion of rejecting reflections with an F/σ of <3.0, the resolution in the a^* direction extended to 2.9 Å, but only to 3.5 Å in the b^* and c^* directions (Figure S1 of the Supporting Information).

Although the ellipsoidally truncated data resulted in significantly improved maps, R-factors were not significantly lowered, and ensuing models were virtually unchanged. A plot of the R-factor as a function of resolution

Table 1: Data Collection and Refinement Statistics

space group	$P2_1$
unit cell	
a (Å)	135.24
b (Å)	94.87
c (Å)	300.89
β (deg)	94.81
no. of molecules per asymmetric unit	2
Matthews coefficient	2.92[a]
highest resolution	3.3 (3.30−3.42)[b]
no. of observations[c]	315232
no. of unique reflections to a resolution of 3.3 Å[c]	107192 (7844)[b]
completeness at a resolution of 3.3 Å (%)	92.6 (68.3)[b]
redundancy	2.9 (2.1)[b]
R_{sym}(I)[d]	0.102 (0.250)[b]
mosaicity (deg)	0.77
no. of reflections submitted for anisotropy correction[e]	165298
no. of reflections removed by truncation	48832
anisotropic truncation resolution (*a**, *b**, *c**)	2.9, 3.5, 0.3.5
no. of reflections used after truncation	116466
isotropic *B* value applied	−28.78
new refinement resolution range (Å)	500−2.9
completeness at a resolution of 2.9 Å (%)	59.9
R-factor[f]	0.250
R_{free}[g]	0.308
rmsd for ideal bond lengths (Å)	0.013
rmsd for bond angles (deg)	1.48
no. of amino acid residues in protein	2881 (2964)[h]
no. of amino acid residues in model (two molecules)	1913, 1947

[a] Based on a MW of 333000 to reflect minor proteolysis. [b] Values in parentheses are for the highest-resolution shell. [c] Measured with Scalepack (*29*). [d] $R_{sym} = (\sum|I - \langle I\rangle|)/(\sum|I|)$. [e] Measured by XDS (*30*) during reprocessing of data for higher-resolution reflections. [f] Crystallographic *R*-factor $= (\sum||F_o| - |F_c||)/(\sum|F_o|)$ with 95% of the native data. [g] R_{free} is the *R*-factor based on 5% of the native data withheld from the refinement. [h] Estimated to reflect minor proteolysis; native value in parentheses.

revealed a spike in the 3.65−3.85 resolution shell, coincident with a spike in the plot of the average intensity versus resolution. The correlation suggested that the measured intensities in this resolution shell were being corrupted by an ice ring that had become accentuated during the anisotropic scaling. Accordingly, the data were completely reprocessed from the starting images using XDS. The erroneously high intensities of reflections in the 3.65−3.85 shell resulting from the ice ring background were dampened by performing a bin-wise scaling (50 bins) of F_o to F_c, each of 50 bins being scaled by a multiplicative constant to F_c. The rationale was that resolution-dependent scaling would minimize discrepancies between F_o and F_c caused by background scattering of the ice. The operation reduced the spike in intensities in the 3.65−3.85 shell, the *R*-factors in this shell dropping from 0.46 to 0.38.

Further refinement with RefMac (*32*) in conjunction with TLS (*40*) at 2.9 Å resulted in the working *R*-factor dropping to 25.2 and the free *R*-factor to 31.6 (Table 1). These values are well within the range of reported *R*-factors in this resolution range (*44*). Although refinement was conducted at 2.9 Å resolution, the strong anisotropy implies that the "effective resolution" was on the order of 3.3 Å.

Quality of the Structure. Periodic PROCHECK evaluations (*43*) were conducted and compared with those for chicken fibrinogen (PDB entry 1M1J), D-dimer (PDB entry 1FZC), and the fragment E region of a thrombin−E complex (PDB entry 2A45) (Table 2). Beyond that, the model naturally differs in quality from sector to sector. The firmly packed globular regions are very well resolved, but the more loosely packed coiled coils are less well resolved. As was the case for the chicken structure, *B*-factors are highest in the middle regions of the coiled coils (Figure S2 of the Supporting Information). On another note, the two different molecules in the asymmetric unit differ, one having better density in some areas and vice versa. A representative section of electron density for a section in the middle of a coiled coil is shown as a simulated annealing omit map in Figure 3A, and another for a region in the γC domain in Figure 3B. A stereo depiction of electron density taken from a $2F_o - F_c$ map around the carbohydrate cluster at Asnβ364 is shown in Figure 4.

Overall Structure. The overall structures of the two molecules in the asymmetric unit are similar to those found previously for chicken and bovine fibrinogens (Figure 5), although, as will be developed further below, there are some significant conformational differences with regard to bending and twisting. A structural overlay of the central region with the fragment E portion of a previously reported thrombin−fragment E complex (*13*) is shown in Figure 6.

The individual chains making up the coiled coils are mostly helical, the major exception being the "out-loop" that occurs in the γ chains between Proγ70 and Proγ76 at virtually the same location as the corresponding departure from helicity in chicken fibrinogen (*18*) (Figure S2 of the Supporting Information). Not unexpectedly, the bending of the coiled coils is most pronounced in those regions with runs of polar amino acids that are uncharacteristic for α helices, in particular, α-chain residues 99−107, β-chain residues 126−131, and γ-chain residues 69−77.

The biantennary carbohydrate cluster that occurs at Asnβ364 was unusually clear, all 11 sugar residues being apparent in three of the clusters where the tips of both "antennae" are involved in obvious contacts, one to Trpβ424 of the same molecule and the other to Hisα84 of a coiled coil on a neighboring molecule. That the visualization of these clusters is due to the vagaries of crystal packing is underscored by the fact that it was possible to place only two sugar residues in the carbohydrate clusters at Asnγ52 in the mobile coiled region where terminal sugar attachments are lacking, and on only one side of the two molecules of the asymmetric unit at that.

There was no discernible electron density corresponding to the αC domains. In this regard, we scoured maps of all kinds at various levels of signal to noise in an effort to identify unassigned clumps of electron density. Similarly, the mobile amino-terminal segments of the α and β chains are not visible in electron density maps, although the symmetrical disulfide connecting the two Cysα28 residues in the dimer was discernible, as were the connections between Cysα36 and Cysβ65.

Crystal Packing. The crystal packing exhibited a variety of unique intermolecular contacts, including a novel antiparallel association of coiled coils from neighboring molecules, an antiparallel contact between βC domains,

Table 2: Comparison of Validations by PROCHECK[a] Analysis

structure	D-dimer	fibrinogen	fibrinogen[b]	fragment E[c]
species	human	chicken	human	human
PDB entry	1FZC	1M1J	3GHG	2A45[c]
no. of residues in model	1366	1988	3918[b]	278[c]
resolution (Å)	2.3	2.7	3.3	3.65
Ramachandran core	83.7	79.4	82.1	75.4
% disallowed	0.3	0.4	0.2	0.4

[a] PROCHECK version 3.5 (*43*). [b] Two molecules in the asymmetric unit. [c] Fragment E portion of the thrombin−E complex.

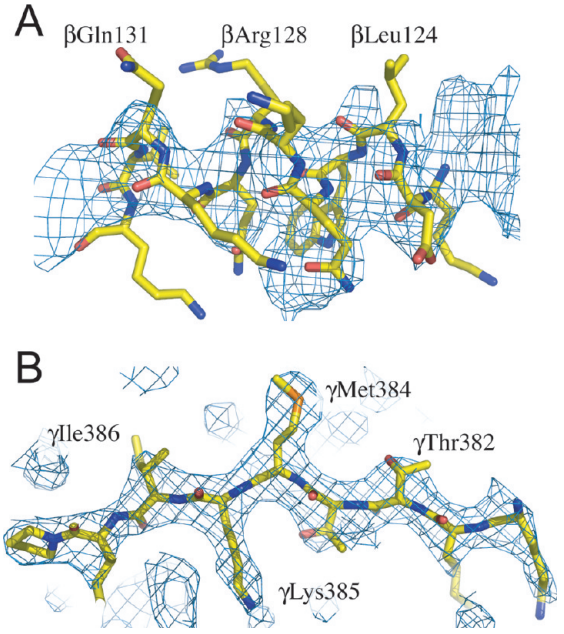

FIGURE 3: Comparison of map quality in poor and good regions. (A) Simulated annealing omit map of a section of β chain (residues 122−133) situated in midsection of a coiled coil calculated at 3.0 Å resolution and contoured at 2.0σ. (B) Simulated annealing omit map of a section of the γC domain (residues 380−390) shown under the same conditions. The peptide segments shown were not included in the calculation of either of the maps.

and a relatively open-face abutment of γ chains at the D−D interface (Figure 7). Perhaps the most unexpected of these was the association of βC domains, the antiparallel association differing from what has been proposed in past models of fibrin formation (*23*) and suggesting that protofibrils may employ antiparallel interactions as well. Also in an antiparallel mode, the coiled coils of neighboring molecules bump up against each other in an interaction involving the nonhelical region of one molecule with a helical region of the other.

Structural Alignments. Two sets of superposed structures were examined. In one, the four half-molecules that occur in the asymmetric unit of human fibrinogen were structurally aligned on the amino-terminal portions of their coiled coils (Figure 8A). In the second, these same structures were aligned with their bovine and chicken counterparts (Figure 8B). The spread of resulting structures defines a minimum envelope of flexibility for the molecule.

With regard to the D−D interface, comparison with a wide variety of previously determined structures for fragments D and D-dimer shows that this interface can slip and slide to a significant degree, also. Significantly, the plane in which these excursions occur coincides with the bending observed in the coiled coils (Figure 9).

DISCUSSION

Although three-dimensional information was already in hand for large portions of the human fibrinogen molecule in the forms of fragment D (*5*), D-dimer (*7*), and fragment E (*13*), the nature of much of the coiled coils had to be inferred from structures of the chicken native molecule (*18*). The current structure now fills that void. In particular, there is a close parallel to the chicken structure in the nonhelical parts of the coiled coils in spite of the very different sequences between species that occur in these regions. It may now be possible to correlate more reliably the abnormal properties of variant human fibrinogens containing mutations in the regions of the coiled coils (*45*), as described more fully below.

Beyond that, the lack of electron density for regions corresponding to the αC domains, often termed "free swimming appendages", is further testimony to the mobile nature of these entities (*46*), elegant NMR studies showing some core structure notwithstanding (*47*, *48*). As were the cases for both native chicken and modified bovine fibrinogen structures, it was possible to trace only the α-chain density of the segment that runs counter to the coiled coils back to α-chain residue 212 which reaches to approximately the midpoint of the coiled coils, even though gel electrophoresis and amino-terminal sequence studies both show that at the least another 350 residues are present in the α chains beyond this point. Even at 2.7 Å resolution, the chicken structure, which was determined from material that was wholly intact and perfectly native, did not reveal the whereabouts of the highly flexible and mobile αC domains. As such, it is not surprising that in this study no density was found that could be assigned to αC domains with any certainty.

Carbohydrate Clusters. Asparaginyl-linked carbohydrate is an integral feature of all vertebrate fibrinogens. In the case of the human protein, biantennary clusters composed of 11 sugar residues each are attached to Asnγ52 and Asnβ364 (*49*). Although the characteristic mobility of such clusters is well-known (*50*), to the point where often only one or two of the sugar residues can be seen in electron density maps, in some situations the idiosyncrasies of crystal packing have allowed a reasonable view. In lamprey fibrinogen fragment D, for example, seven of the 11 sugar residues were positioned for the βC carbohydrate cluster (*10*). Now, in the human fibrinogen structure, it has proven to be possible to position all 11 residues for three of the four Asnβ364 clusters that occur in the asymmetric unit (Figure 4). The positioning is functionally significant because the cluster lies adjacent to the βC hole (Figure 7) and must hinder access to the flexibly tethered B knobs of neighboring molecules during fibrin formation. At first glance, the observation might seem to provide support for early findings that deglycosylation of fibrinogen results in accelerated fibrin formation (*51*). However, the fact that simple desialidation gives rise to the same acceleration of polymeri zation (*52*) makes it more likely that an electrostatic charge effect is the dominant force behind the speedier

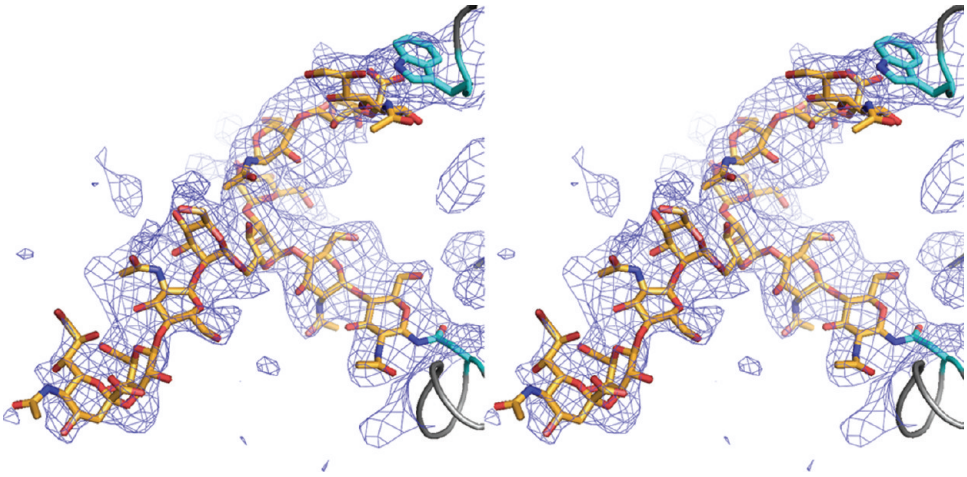

FIGURE 4: Stereo depiction of electron density representing a carbohydrate cluster attached to Asnβ364. All 11 known sugar residues are shown in the model. The map, shown at 3.3 Å resolution and contoured at 1.2σ, was calculated with $2F_o - F_c$ coefficients and may have some model bias.

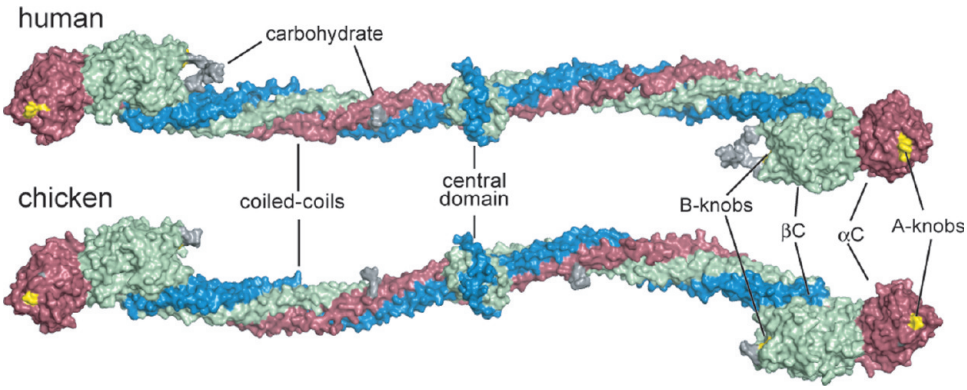

FIGURE 5: Space-filling models of the human fibrinogen molecule (top) compared with the previously reported chicken structure (bottom): α chains, green; β chains, blue; γ chains, red; synthetic peptide knobs, yellow; carbohydrate, gray.

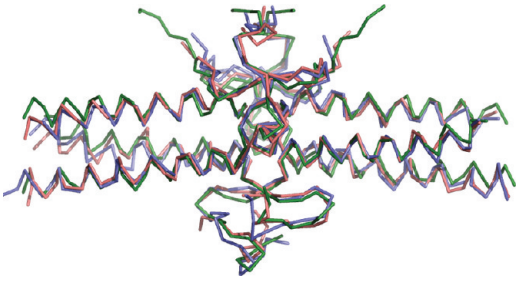

FIGURE 6: Superposition of central regions of the two molecules of human fibrinogen (red and blue) with the corresponding structure reported for the fragment E region of a thrombin–fragment E complex (green) (*13*) (PDB entry 2A45). The rmsd between the two molecules in the current structure is 1.1, and the rmsd between both of those and fragment E is 1.6.

polymerization observed upon deglycosylation, and the hindrance for the B knob may have subtler implications, including delaying the formation of binding sites for t-PA and plasminogen (*24*).

Flexibility of Coiled Coils. It has long been supposed that the coiled-coil regions of fibrinogen molecules must afford a degree of flexibility, both to the individual molecules and to fibrin strands (*53*). In particular, it was conjectured that, although those segments of the coiled coils that are fully α helical might be stiff, those regions with nonhelical components, and which are primary targets during fibrinolysis (*54*), would constitute a "flexible hinge" (*53*). Moreover, the fact that fibrin gels exhibit both compressible and extensible properties was well explained by the coiled coils acting as "inter-domainal springs" (*53*).

The determination of the crystal structure of modified bovine fibrinogen led to the resurrection of the notion of the flexible hinge (*20*). The four unique coiled-coil regions of the bovine structure are bent to various degrees, both in the plane of and perpendicular to the sigmoidal axis (*20*). Similarly, the two coiled-coil regions of chicken fibrinogen are bent relative to each other, mostly within the plane of the sigmoidal axis in this case (*17*).

As was the case for bovine fibrinogen, the structure reported here has two molecules per asymmetric unit; both molecules differ measurably in the flex of the coiled coils from the bovine and the chicken models and are bent to different extents, mostly perpendicular to the sigmoidal plane. Superposition of all 10 unique coiled-coil regions (two from chicken and four each from bovine and human) shows how readily packing forces can distort the coiled-coil regions from their canonical form; the resulting collection of forms likely reflects the minimum limits of conformational flexibility in solution (Figure 8).

Associated Coiled Coils. Two of the best known variant human fibrinogens in the coiled-coil section of the molecule are the result of three-base (single-amino acid) deletions that are thought to disrupt α helicity. Fibrinogen

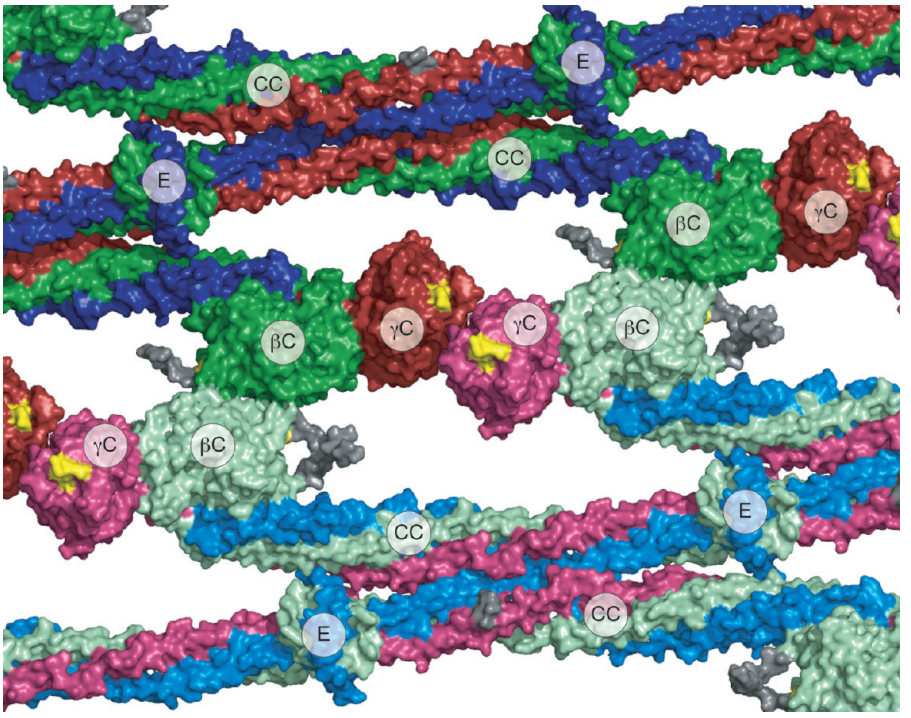

FIGURE 7: Crystal packing contacts in crystals of human fibrinogen, including end-to-end interactions of γC domains, lateral antiparallel interaction of βC domains, and antiparallel association of coiled coils (cc). The labeled features include several carbohydrate clusters (gray), as well as A and B knobs (yellow) bound in γC and βC holes. α chains are colored green, β chains blue, and γ chains red. The central domain is denoted by a circled E. Lighter and darker color shades distinguish the two crystallographically unique molecules.

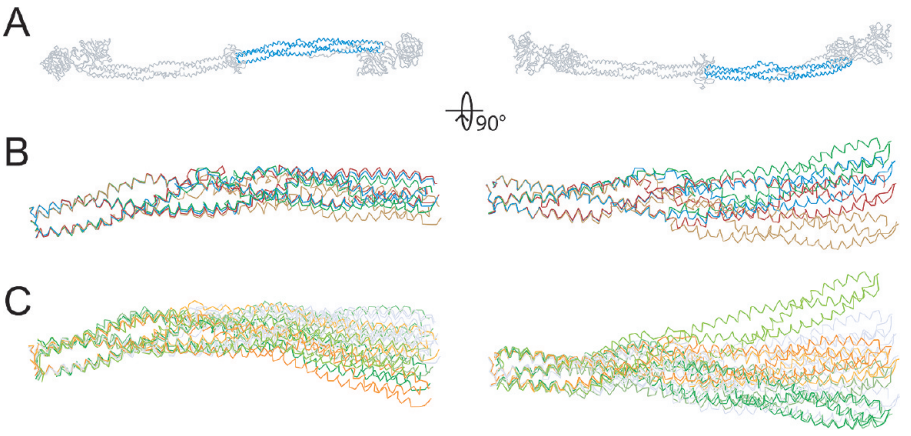

FIGURE 8: Differences in bending and twisting of coiled coils. (A) Two views of the human fibrinogen molecule with one set of coiled coils highlighted in blue in each case; the left view is in the sigmoidal plane. (B) Structural alignment of coiled-coil regions of four half-molecules in the asymmetric unit of human fibrinogen when aligned on 25 amino-terminal residues of each chain. (C) Structural alignment of 10 unique coiled-coil domains from human (four half-molecules), bovine (four half-molecules), and chicken (two half-molecules) showing the extent of flex in coiled-coil regions. The human structures are colored gray, bovine structures (PDB entry 1DEQ) in shades of green, and chicken structures (PDB entry 1M1J) in shades of orange. In both alignment sets, the flexibility is significantly greater perpendicular to the sigmoidal plane than within the plane.

Caracas VI lacks Asnα80 (*55*), and fibrinogen Kyoto IV lacks Serβ111 (*56*); both exhibit defective fibrin formation, fibrinogen Kyoto IV in particular exhibiting enhanced lateral association during fiber formation.

Coincidentally, both of these locations (Asnα80 and Serβ111) not only occur within the same extended all-polar region in the coiled coil but also are adjacent to the carbohydrate attachment point at Asnγ52. This region is a "touch point" where the coiled coils from different molecules associate in an antiparallel fashion in the crystal (Figure 7). It is not impossible that these kinds of associations between coiled coils may also occur in fibrin.

Flexibility at the D−D Interface. The packing between ends of individual fibrinogen molecules in crystals has strong implications for fibrin formation. When the first crystal structures of a fragment D-dimer from factor XIII-cross-linked fibrin were determined, the $\gamma-\gamma$ interface between fibrin monomer units was found to be offset and asymmetric (*5*). Thus, in one direction, the residue Argγ275 is directed toward Serγ300 on the other side of the interface, but in the opposite direction, Argγ275 is directed toward Tyrγ280. The two asymmetrically abutting molecules were arbitrarily designated A and B (*5*).

The same general kind of abutment has since been found in the crystal structures of all D fragments,

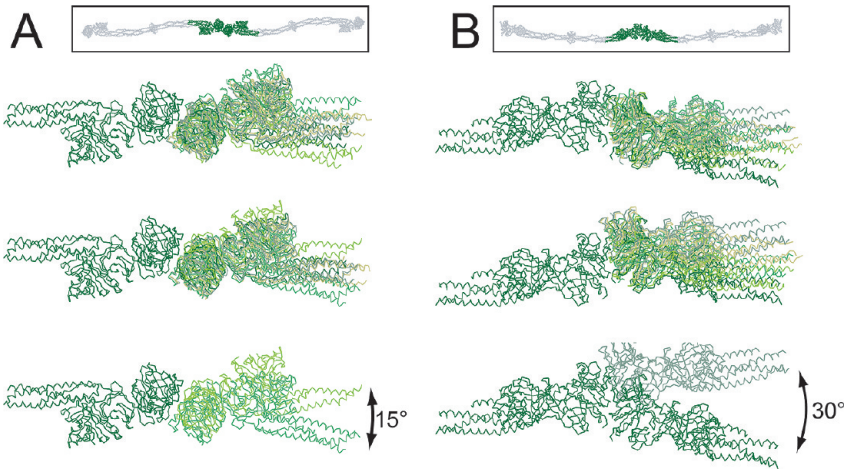

FIGURE 9: Variability in end-to-end packing at the D−D interface for various structures of fibrinogen, fragment D, and D-dimer. The two insets at the top show end-to-end packing in human fibrinogen crystals from two orthogonal views, with the region of comparison highlighted in green. Views shown are (A) within the sigmoidal plane and (B) perpendicular to the plane. In the topmost panels, the structures of bovine fibrinogen (PDB entry 1DEQ), chicken fibrinogen (PDB entry 1M1J), human fragment D (PDB entry 1FZA), and human fragment D-dimer (PDB entry 1FZC) were each aligned with human fibrinogen using the γC domains of molecule A as defined in ref *5*. The same structures are aligned using the γC domains of molecule B in the middle row. The bottommost alignments are limited to those structures showing the most extreme differences in each plane: bovine and chicken fibrinogen within the sigmoidal plane and human fibrinogen and human D-dimer perpendicular to the plane. In all cases, the domain used for aligning is on the left.

D-dimer, and fibrinogens that have been determined to date. Models of overlapping units in the form of protofibrils were readily constructed (*5*, *22*), and the arrangement has been presumed to be what occurs in native fibrin. It is not a tightly associated arrangement, however, and there is a curious lack of specific interactions between the two D units. Still, it easily accommodates a set of closely tethered "A knobs", the γ-chain "holes" of abutting molecules being approximately 22 Å apart. The interface is also in accord with known variant human fibrinogens, an especially a large number of which involve Argγ275 and exhibit defective fibrin formation (*45*).

As the number of crystal structures of fragments D and D-dimer has grown over the years, it has become clear that there are somewhat different versions of this interface, likely the result of distortions caused by crystal packing (*8*, *12*). Apparently, the D−D interface can slip and slide with little consequence. The interface found in human fibrinogen crystals is of a type found in D-dimer cocrystallized with assorted peptides (PDB entry H1N86) (*11*) and also a fragment D cocrystallized with GPRPam alone (PDB entry 2HPC). The hole-to-hole distances in these various forms differ only slightly one to another, indicating that all can accommodate pairs of tethered A knobs from companion molecules in fibrin.

Significantly, these D−D interface "distortions," or alternative arrangements, are mainly restricted to a single plane and are complementary to the flexibility observed in the variously bent coiled coils (Figure 9).

Distensibility of Fibrinogen and Fibrin. Of late, there has been renewed interest in the matter of the flexibility not only of fibrinogen but also of fibrin. Indeed, fibrin has been found to be among the most flexible of naturally occurring fibers (*57*), and impressive experiments employing single-molecule atomic force microscopy have sought to measure the distensibility of both fibrinogen (*58*) and fibrin (*59*). Simulation studies designed to demonstrate the inherent elasticity of fibrinogen coiled coils have also been conducted (*59*), the chicken fibrinogen model (*18*) being used as a starting point.

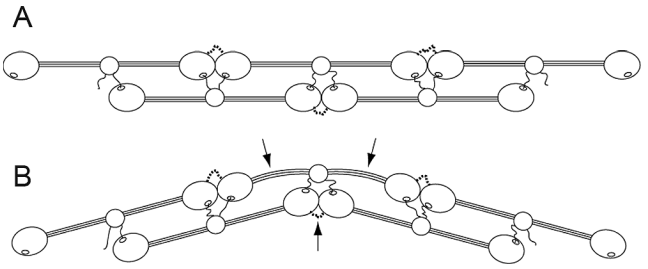

FIGURE 10: Cartoon showing that flexible regions in coiled-coil regions of fibrin are complemented by slipping and sliding at the D−D interfaces. Arrows indicate distortions that are correlated in coiled coils and the D−D interface. Broken lines denote covalent cross-links incorporated by factor XIII between abutting γ chains, which themselves have been shown to be flexible (*11*).

Although the coiled coils have been the central focus of such studies, the slipping and sliding of D−D interfaces observed in different crystal forms of human fibrinogen and its fragments suggests that the coiled coils are not the only locations in fibrin where flexible linkages occur (Figure 10). These observations are also consistent with the flexible nature of $\gamma-\gamma$ cross-links, which have been shown to be sufficiently mobile that a pair of cross-linked D domains can shift from one kind of interface to another with the cross-link remaining intact (*11*). It is altogether likely that fibrin fibers and the protofibrils of which they are made depend on these flexible "joints," as well as the springiness of coiled coils, to relieve the stresses and strains that natural clots must experience in vivo.

ACKNOWLEDGMENT

We thank Nick Nguyen of the UCSD X-ray Facility and Corey Ralston at ALS for their assistance during our visits.

SUPPORTING INFORMATION AVAILABLE

Plot of F/σ versus resolution obtained from an anisotropy server showing significant diffraction out to 2.9 Å in the a^* direction (Figure S1). Plot of *B*-factors versus amino acid sequence showing peaks in the middle of three-stranded coiled coils (Figure S2). The regions shown begin at the first cysteine residues of disulfide ring 1 (DSR1) and end at the second cysteine of disulfide ring 2 (DSR2). An "out-loop" region in γ chains occurs at the same place as in chicken fibrinogen. Blue, α chain; green, β chain; red, γ chain. This material is available free of charge via the Internet at http://pubs.acs.org.

REFERENCES

1. Scheraga, H. A., and Laskowski, M.Jr. (1957) The fibrinogen-fibrin conversion. *Adv. Protein Chem. 12*, 1–131.
2. Doolittle, R. F. (1973) Structural aspects of the fibrinogen to fibrin conversion. *Adv. Protein Chem. 27*, 1–109.
3. Weisel, J. (2006) Fibrinogen and fibrin. *Adv. Protein Chem. 77*, 247–299.
4. Yee, V. C., Pratt, K. P., Cote, H. C., LeTrong, I., Chung, D. W., Davie, E. W., Stenkamp, R. E., and Teller, D. C. (1997) Crystal structure of a 30 kDa C-terminal fragment from the γ chain of human fibrinogen. *Structure 5*, 125–138.
5. Spraggon, G., Everse, S. J., and Doolittle, R. F. (1997) Crystal structures of fragment D from human fibrinogen and its crosslinked counterpart from fibrin. *Nature 389*, 455–462.
6. Spraggon, G., Applegate, D., Everse, S. J., Zhang, J.-Z., Veerapandian, L., Redman, C., Doolittle, R. F., and Grieninger, G. (1998) Crystal structure of a recombinant α_EC domain from human fibrinogen-420. *Proc. Natl. Acad. Sci. U.S.A. 95*, 9099–9104.
7. Everse, S. J., Spraggon, G., Verrapandian, L., Riley, M., and Doolittle, R. F. (1999) Crystal structure of fragment double-D from human fibrin with two different bound ligands. *Biochemistry 38*, 2941–2946.
8. Everse, S. J., Spraggon, G., Veerapandian, L., and Doolittle, R. F. (1999) Conformational changes in fragments D and double-D from human fibrin(ogen) upon binding the peptide ligand Gly-His-Arg-Pro-amide. *Biochemistry 38*, 2941–2946.
9. Madrazo, J., Brown, J. H., Litvinovich, S., Dominguez, R., Yakovlev, S., Medved, L., and Cohen, C. (2001) Crystal structure of the central region of bovine fibrinogen (E5 fragment) at 1.4 angstroms resolution. *Proc. Natl. Acad. Sci. U.S.A. 98*, 11967–11972.
10. Yang, Z., Spraggon, G., Pandi, L., Everse, S. J., Riley, M., and Doolittle, R. F. (2002) Crystal structure of fragment D from lamprey fibrinogen complexed with the peptide Gly-His-Arg-Pro-amide. *Biochemistry 41*, 10218–10224.
11. Yang, Z., Pandi, L., and Doolittle, R. F. (2002) The crystal structure of fragment double-D from cross-linked lamprey fibrin reveals isopeptide linkages across an unexpected D−D interface. *Biochemistry 41*, 15610–15617.
12. Kostelansky, M. S., Betts, L., Gorkkun, O. V., and Lord, S. T. (2002) 2.8 Å crystal structures of recombinant fibrinogen fragment D with and without two peptide ligands: GHRP binding to the "b" site disrupts its nearby calcium-binding site. *Biochemistry 41*, 12124–12132.
13. Pechik, I., Madrazo, J., Mosesson, M., Hernandez, I., Gilliland, G. J., and Medved, L. (2004) Crystal structure of the complex between thrombin and the central "E" region of fibrin. *Proc. Natl. Acad. Sci. U.S.A. 101*, 2718–2723.
14. Kostelansky, M. S., Bollinger-Stucki, B., Betts, L., Gorkun, O. V., and Lord, S. T. (2004) BβGlu397 and BβAsp398 but not BβAsp432 are required for "B:b" interactions. *Biochemistry 43*, 2465–2474.
15. Doolittle, R. F., Chen, A., and Pandi, L. (2006) Differences in binding specificity for the homologous γ- and β-chain "holes" on fibrinogen: Exclusive binding of Ala-His-Arg-Pro-amide by the β-chain hole. *Biochemistry 45*, 13962–13969.
16. Doolittle, R. F., and Pandi, L. (2007) Probing the β-chain holes of fibrinogen with synthetic peptides that differ at their amino termini. *Biochemistry 46*, 10033–10038.
17. Yang, Z., Mochalkin, I., Veerapandian, L., Riley, M., and Doolittle, R. F. (2000) Crystal structure of native chicken fibrinogen at 5.5 Å resolution. *Proc. Natl. Acad. Sci. U.S.A. 97*, 3907–3912.
18. Yang, Z., Kollman, J. M., Pandi, L., and Doolittle, R. F. (2001) Crystal structure of a native chicken fibrinogen at 2.7 Å resolution. *Biochemistry 40*, 12515–12523.
19. Weissbach, L., and Grieninger, G. (1990) Bipartite mRNA for chicken α-fibrinogen potentially encodes an amino acid sequence homologous to β- and γ-fibrinogens. *Proc. Natl. Acad. Sci. U.S.A. 87*, 5198–5202.
20. Brown, J. H., Volkmann, N., Jun, G., Henschen-Edman, A., and Cohen, C. (2000) The crystal structure of modified bovine fibrinogen. *Proc. Natl. Acad. Sci. U.S.A. 97*, 85–90.
21. Doolittle, R. F. (2003) Some notes on crystallizing fibrinogen and fibrin fragments. *Biophys. Chem. 100*, 307–313.
22. Williams, R. C. (1981) Morphology of bovine fibrinogen and fibrin polymers. *J. Mol. Biol. 150*, 399–408.
23. Yang, Z. (2000) A model of fibrin formation based on crystal structures of fibrinogen and fibrin fragments complexed with synthetic peptides. *Proc. Natl. Acad. Sci. U.S.A. 97*, 14156–14161.
24. Doolittle, R. F., and Pandi, L. (2006) Binding of synthetic B knobs to fibrinogen changes the character of fibrin and inhibits its ability to activate tissue plasminogen activator and its destruction by plasmin. *Biochemistry 45*, 2657–2667.
25. Merrifield, R. B. (1964) Solid phase peptide synthesis. 3. An improved synthesis of bradykinin. *Biochemistry 3*, 1385–1390.
26. Doolittle, R. F., Schubert, D., and Schwartz, S. A. (1967) Amino acid sequence studies on artiodactyls fibrinopeptides. I. Dromedary camel, mule deer and Cape Buffalo. *Arch. Biochem. Biophys. 118*, 456–467.
27. Finlayson, J. S., and Mosesson, M. W. (1963) Heterogeneity of human fibrinogen. *Biochemistry 2*, 42–46.
28. Mosesson, M. W., Finlayson, J. S., Umfleet, R. A., and Galanakis, D. (1972) Human fibrinogen heterogeneities. I. Structural and related studies of plasma fibrinogens which are high solubility catabolic intermediates. *J. Biol. Chem. 247*, 5210–5219.
29. Otwinowski, Z., and Minor, W. (1997) Processing of X-ray diffraction data collected in oscillation mode. *Methods Enzymol. 276*, 307–326.
30. Kabsch, W. (1993) Automatic processing of rotation diffraction data from crystals of initially unknown symmetry and cell contants. *J. Appl. Crystallogr. 26*, 795–800.
31. Navaza, J. (2001) Implementation of molecular replacement in AmoRe. *Acta Crystallogr. D57*, 1367–1372.
32. Collaborative Computational Project Number 4 (1994) *Acta Crystallogr. D50*, 760–763.
33. McCoy, A. J., Grosse-Kunstleve, R. W., Storone, L. C., and Read, R. J. (2005) Likelihood-enhanced fast translation functions. *Acta Crystallogr. D61*, 458–464.
34. Jones, T. A., Zou, J.-Y., Cowan, S. W., and Kjeldgaard, M. (1991) Improved methods for building protein models in electron density maps and the location of errors in these models. *Acta Crystallogr. A47*, 110–119.
35. Brunger, A. T., Adams, P. D., Chlore, G. M., DeLano, W. L., Gros, P., Grosse-Kunstleve, R. W., Jiang, J.-S., Kuszewski, J., Nilges, M., Pannu, N. S., Read, R. J., Rice, L. M., Simonson, T., and Warren, G. L. (1998) Crystallography and NMR system: A new software suite for macromolecular structure determination. *Acta Crystallogr. D54*, 905–921.
36. Murshudov, G. N., Vagin, A. A., and Dodson, E. J. (1997) Refinement of macromolecular structures by the maximum-likelihood method. *Acta Crystallogr. D53*, 240–255.
37. Hodel, A., Kim, S.-H., and Brunger, A. T. (1992) Model bias in macromolecular crystal structures. *Acta Crystallogr. A48*, 851–858.
38. Delano, W. L. (2002) *The PyMOL Molecular Graphics System*, DeLano Scientific, San Carlos, CA..
39. Strong, M., Sawaya, M. R., Wang, S., Phillips, M., Cascio, D., and Eisenberg, D. (2006) Toward a structural genomics of complexes: Crystal structure of a PE/PPE protein complex from *Mycobacterium tuberculosis*. *Proc. Natl. Acad. Sci. U.S.A. 103*, 8060–8065.
40. Winn, M. D., Isupov, M. N., and Murshudov, G. N. (2001) Use of TLS parameters to model anisotropic displacements in macromolecular refinement. *Acta Crystallogr. D57*, 122–133.
41. Painter, J., and Merritt, E. A. (2006) TLSMD web server for the generation of multi-group TLS models. *J. Appl. Crystallogr. 39*, 109–111.
42. Emsley, P., and Cowtan, K. (2004) Coot: Model-building tools for molecular graphics. *Acta Crystallogr. D60*, 2126–2132.
43. Laskowski, R. A., MacArthur, M. W., Moss, D. S., and Thornton, J. M. (1993) PROCHECK: A program to check the stereochemical quality of protein structures. *J. Appl. Crystallogr. 26*, 283–291.

44. Read, R. J., and Kleywegt, G. J. (2009) Case-controlled stucture validation. *Acta Crystallogr. D65*, 140–147.
45. Hanss, M., and Biot, F. (2001) A database for human fibrinogen variants. *Ann. N.Y. Acad. Sci. 936*, 89–90.
46. Doolittle, R. F., and Kollman, J. M. (2006) Natively unfolded regions of the vertebrate fibrinogen molecule. *Proteins 63*, 391–397.
47. Burton, R. A., Tsurupa, G., and Medved, L..; et al. (2006) Identification of an ordered compact structure within the recombinant bovine fibrinogen αC domain fragment by NMR. *Biochemistry 45*, 2257–2266.
48. Burton, R. A., Tsurupa, G., and Hantgan, R. R..; et al. (2007) NMR solution structure, stability and interaction of the recombinant bovine fibrinogen αC domain fragment. *Biochemistry 46*, 8550–8560.
49. Townsend, R. R., Hilliker, E., Li, Y.-T., Laine, R. A., Bell, W. R., and Lee, Y. C. (1982) Carbohydrate structure of human fibrinogen. *J. Biol. Chem. 257*, 9704–9710.
50. Wu, P., Lee, K. B., Lee, Y. C., and Brand, L. (1996) Solution conformations of a biantennary glycopeptide and a series of its exoglycosidase products from sequential trimming of sugar residues. *J. Biol. Chem. 271*, 1470–1474.
51. Langer, B. G., Weisel, J. W., Dinauer, P. A., Nagaswami, C., and Bell, W. R. (1988) Deglycosylation of fibrinogen accelerates polymerization and increases lateral aggregation of fibrin fibers. *J. Biol. Chem. 263*, 15056–15063.
52. Okude, M., Yamanaka, A., Morimoto, Y., and Akihama, S. (1993) Sialic acid in fibrinogen: Effects of sialic acid on fibrinogen-fibrin conversion by thrombin and properties of asialofibrin clot. *Biol. Pharm. Bull. 16*, 448–452.
53. Doolittle, R. F., Goldbaum, D. M., and Doolittle, L. R. (1978) Designation of sequences involved in the "coiled-coil" interdomainal connections if fibrinogen: Construction of an atomic scale model. *J. Mol. Biol. 120*, 311–325.
54. Doolittle, R. F., Cassman, K. G., Cottrell, B. A., Friezner, S. J., and Takagi, T. (1977) Amino acid sequence studies on the α chain of human fibrinogen. Covalent structure of the α-chain portion of fragment D. *Biochemistry 16*, 1710–1715.
55. Marchi, R. C., Meyer, M. H., de Bosch, N. B., Arocha-Pinango, C. L., and Weisel, J. W. (2004) A novel mutation (deletion of Aα-Asn 80) in an abnormal fibrinogen: Fibrinogen Caracas VI. Consequences of disruption of the coiled-coil for the polymerization of fibrin: Peculiar clot structure and diminished stiffness of the clot. *Blood Coagulation Fibrinolysis 15*, 550–567.
56. Okumura, N., Terasawa, F., Hirota-Kawadobora, M., Yamauchi, K., Nakanishi, K., Shia, S., Ichiyama, S., Saito, M., Kawai, M., and Nakahata, T. (2005) A novel variant fibrinogen, deletion of Bβ111Ser in coiled-coil region, affecting lateral aggregation. *Clin. Chim. Acta 365*, 160–167.
57. Guthold, M., Liu, W., Sparks, E. A., Jawert, L. M., Peng, L., Falvo, M., Superfine, R., Hantgan, R. R., and Lord, S. T. (2007) A comparison of the mechanical and structural properties of fibrin fibers with other protein fibers. *Cell Biochem. Biophys. 49*, 165–181.
58. Brown, A. E., Litvinov, R. I., Discher, D., and Weisel, J. W. (2007) Forced unfolding of coiled-coils in fibrinogen by single-molecule AFM. *Biophys. J. Lett. 92*, L09–L41.
59. Lim, B. B., Lee, E. H., Sotomeyer, M., and Schulten, K. (2007) Structural basis of fibrin clot elasticity. *Structure 16*, 449–459.
60. Medved, L., and Weisel, J. W. (2009) Recommendations for nomenclature on fibrinogen and fibrin. *J. Thromb. Haemostasis 7*, 355–359.